Active distance stabilization of large bodies using Fabry-Perot interferometry

Enrico Canuto
Dipartimento di Automatica e Informatica, Politecnico di Torino
Corso Duca degli Abruzzi 24, 10129 Torino,Italy
enrico.canuto@polito.it

Abstract

The paper presents control design and results of a distance stabilization experiment aiming at picometer repeatability. The experiment, called COSI, was funded by European Space Agency in view of space telescopes needing picoradian precision. Stabilization is achieved by actively controlling the optical length of in vacuum Fabry-Perot interferometers. Experiments stabilized three 0.5m distances between two 7kg plates with a repeatability better than 3pm (1σ), in presence of severe environment noise and artificial micrometer displacements, thus demonstrating feasibility of COSI concept and technology.

1 Introduction

The paper presents the control design and results of an experiment in the active geometry stabilization of large bodies, aiming at picometer repeatability (10^{-12}m). The experiment, called COSI (Control Optics Structure Interaction), was funded by the European Space Agency in view of future space telescopes needing picoradian precision. It was performed on a ground test-bed (Figure 1) enclosed in a vacuum chamber of about 1m^3 volume, partly emulating space conditions.

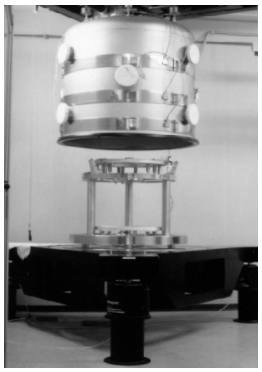

Figure 1: COSI test-bed with the bell-shaped protection

A key technology to be investigated was laser interferometry, based on Fabry-Perot (FP) cavities, as a mean for creating ultra-stable links in large and complex structures. FP cavities having ultra-stable length are commonly employed in dimensional metrology [2] as references in the active stabilization of laser wavelengths. FP cavities can be operated the other way round: by injecting a frequency-stabilized light beam, they become sensors capable of revealing length variations well below the sub-nanometric range and with response times much shorter than milliseconds. A Fabry-Perot interferometer (FPI) is nothing more than two well aligned mirrors with high reflectivity (reflectors). The laser light penetrates the first mirror and is reflected by the second mirror. As the reflected wavefront reaches the first mirror, it is combined with the laser beam through the first mirror. Depending on the phase, the interference may be constructive or destructive. The phase is regulated by varying the cavity optical length. When the cavity length is an integer multiple of half the wavelength of the incoming light, the cavity is said to be *resonant* and no light is reflected out by the cavity. By detecting the intensity of the reflected light in a photo-detector, an error signal proportional to cavity length variation (often called *cavity detuning*) is generated. The error signal is then feed back to a control unit for stabilizing the cavity length through a displacement actuator. To detect the sign of the length variation, the incoming light has to be phase modulated and the photo-detector signal must be demodulated (Pound-Drever technique [4]). A typical set-up is shown in Figure 2.

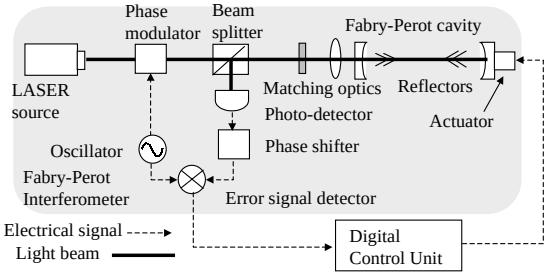

Figure 2: Layout for locking a Fabry-Perot interferometer

A further technology to be investigated, although less critical, was piezo-electric ceramic (typically PZT) as a high-resolution displacement actuator to be employed in a tip-tilt mechanism capable of stabilizing massive bodies along three (or more) Degrees-of-Freedom. Because in dimensional metrology FP cavities are usually stabilized by analog loops, Digital Control Units (DCU) were investigated as alternative stabilizing loops. As a matter of fact digital control was a key factor of the experiment success. The experiment stabilized three 0.5m distances between two circular plates having 0.6m diameter and 7kg mass, emulating large mirrors of space telescopes. Stabilization was achieved with an average error less than 3pm (1σ). The paper is completely dedicated to digital control design and results.

2 Stabilization requirements and fine model

2.1 Stabilization requirements

The problem was to keep two 0.5m distant circular plates rigidly connected by actively stabilizing the optical lengths $L_j(t), j = 1, 2, 3$, of three Fabry-Perot interferometers (Figure 3). Each FPI includes a cavity made by a pair of optical reflectors mounted on each plate and resonating at an integer multiple $N_j \simeq 10^6$ of the half-wavelength $\lambda_0/2 = 532$nm of a laser source. The detuning $\Delta L_j(t)$ of each cavity length with respect to a resonant length $L_{j,0} = N_j\lambda_0/2$ is the variable to be controlled to zero for stabilizing the three plates relative motions, vertical motion z and two tilt angles. Cavity detuning is detected by a suitable electronics providing an error signal $e_j(t)$ which is proportional to $\Delta L_j(t)$ only in a very small range (< 5nm) around resonant lengths. DCU must shift cavity lengths near a resonating length (*recovery*) and then keep the error signal to zero (*stabilization*). The error signal in such a small range can be made equal, by calibration, to cavity detuning up to a measure error η_j: $e_j(t) = \Delta L_j(t) + \eta_j(t)$.

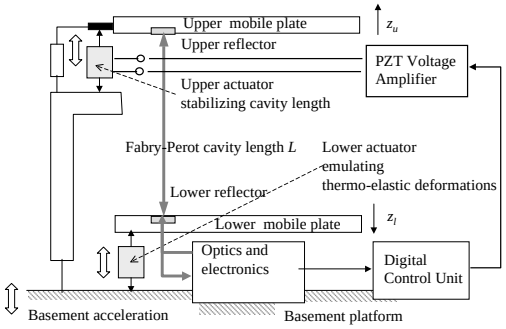

Figure 3: One-third of the stabilized structure

Requirements on tip/tilt stabilization were derived from the active stabilization system of a future space telescope (GAIA-Global Astrometric Interferometer for Astrophysics) aiming at measuring star coordinates of one billion of stars with an accuracy of 10 μarcsec. Parasitic optics tip/tilt movements, mainly due to thermo-elastic deformations, shall be reduced to be less than 20prad (1σ) and in terms of distance variation less than 10pm. Residual optics movements must be averaged over $\tau_0 = 0.75$s to account for the star image integrating time of the detection device. By denoting with $e_j(i)$ the sampled control error ($f_c = 1$kHz) of each distance $j = 1, 2, 3$ to be actively controlled and with $\underline{e}_j(i) = (\sum_{i=1}^{M} e_j(i))/M$ its moving average taken over $M = f_c\tau_0 = 781$ samples, stabilization requirement, expressed as RMS distance variation, amounts to

$$\underline{\sigma}_{e,j} = \sqrt{\mathcal{E}\{\underline{e}_j^2(i)\}} \leq 10pm \; \forall j \qquad (1)$$

Distance stabilization of large bodies in space and on the ground are subject to different constraint. On the ground, relative motion between the actuated body (upper plate) and the reference body (lower plate) can be written as the composition of independent motions z_u and z_l with respect to an inertial frame, made by a rigid and massive basement. Stabilization is achieved by commanding the actuated body to track the motion of the reference one, the latter being modeled as a disturbance to be compensated. FP cavity detuning $\Delta L_j(t)$ can then be written as the sum of the inertial motions of the upper and lower reflectors: $\Delta L_j(t) = z_{u,j}(t) + z_{l,j}(t)$. In space, body motion becomes more or less interacting through supporting structures. Command-to-measure dynamics may become multivariable and subject to interaction uncertainty. COSI experiments were not intended to afford interaction problems, although in the sub-nanometric range basements cannot be supposed rigid.

A further difference concerns basement acceleration sources. In space they are mainly due to moving parts necessary for attitude control. Suitable actuators may reduce them to acceptable levels. Ground sources are

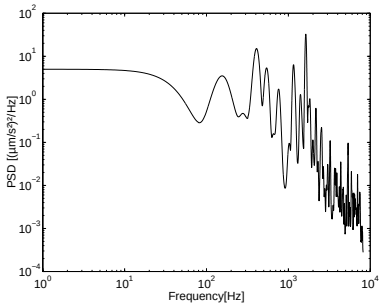

Figure 4: The PSD $S_a^2(f)$ of the basement acceleration

instead stronger and uncontrollable, and although their effect was partly alleviated by isolation supports, COSI test-bed was exposed to a wide-band (> 1kHz) acceleration noise transmitted via ground and acoustic

paths. Its Power Spectral Density (PSD) $S_a(f)$, valid in quiet day hours, is shown in Figure 4 and is bounded by $\underline{S}_a \simeq 2.3(\mu\text{m/s}^2)/\sqrt{\text{Hz}}$. One of the major control problem was that noise, because of aliasing, could spill excessive high-frequency components within control bandwidth. To this end, DCU was designed around a simple but effective digital anti-aliasing filter.

The last problem concerns emulation of space-born thermo-elastic deformations. The main sources are variable solar radiation and internal power dissipation. Since GAIA payload will be revolving and shielded, the main source is due to payload electronics causing distance variations ΔL up to 0.1μm and deformation rates $\dot{L}(t)$ up to 100pm/s. Their attenuation below target repeatability expressed by (1) would not require a control bandwidth larger than 0.1Hz. But also in their respect more severe requirements were adopted for COSI experiment by raising thermo-elastic deformation range and rate to

$$|\Delta L(t)| \leq 1\mu\text{m}, |\dot{L}(t)| \leq 0.1\mu\text{m/s} \qquad (2)$$

2.2 The fine model: the FPI response

The first design step was the development of a *fine* dynamic model based on test-bed design data and structural analysis. To simulate realistic input-output dynamics the following components were carefully modeled: (i) FP interferometers, (ii) vibration modes of plates and supporting structure, (iii) PZT hysteresis and creep (not treated here), (iv) basement acceleration.

Consider a single FPI and denote by $E(t) = E_0 e^{j(\omega_0 t + \beta \sin \Omega t)}, \omega_0 = 2\pi c/\lambda_0$ the phase-modulated radiation incident on the entrance reflector where c is the light speed, $f_m = \Omega/(2\pi) = 2.5$MHz is the modulation frequency, $\lambda_0 = 1064$nm is the laser wavelength and $\beta \simeq 1$ is the modulation amplitude. It can be shown [1] that the reflected light intensity collected as a current $I(t)$ by a photodiode can be developed as an harmonic series $I(t) = I_0(t) + I_{1s}(t)\sin\Omega t + I_{1c}(t)\cos\Omega t + \ldots$. The time-varying coefficients of the series depend on the cavity transfer function

$$H(\omega, t) = -\frac{R(1 - e^{-j\omega\tau})}{1 - R^2 e^{-j\omega\tau}}, \; \tau(t) = 2\frac{L_0 + \Delta L(t)}{c}, \quad (3)$$

expressing time-delay and attenuation of the reflected cavity radiation. In (3), $R = 0.985$ is the average cavity reflectivity and $\tau(t)$ is the round trip time of the light inside the cavity. According to Pound-Drever technique [4], the current $I(t)$ must be demodulated for providing a voltage signal $V(t)$ proportional to the amplitude $I_{1s}(t)$ of the in-phase first-order component. The static relation $V(t) = h(\Delta L(t))$ defines the *interferometer response*, which, highly non-linear, repeats periodically every half-wavelength $\lambda_0/2 = 532$nm. Only in a small range (Figure 5) around resonant lengths, the response, being a monotonic function of $\Delta L(t)$, provides a useful measure to DCU. Within such a range, called *linear range* and limited by $|\Delta L(t)| < \Delta L_{max} = 2.5$nm, the response can be approximated as

$$V(t) \simeq -2a_{1s}\text{Im}H(\omega_0, t) \simeq k_V \mathcal{F}\frac{2\Delta L(t)}{\lambda_0} \qquad (4)$$

where $\mathcal{F} = \frac{\pi R}{1-R^2} \simeq 100$ is the cavity *finesse*. DCU

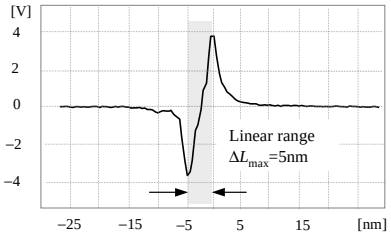

Figure 5: The linear range of the interferometer response

must keep the error signal within the linear range (stabilization) and guarantee that the average error be less than 1/250th of the linear range itself. A second control task must lock cavities to within the linear range at the onset and in case of shocks (recovery).

2.3 The fine model: structural vibration modes

Structural analysis showed that the most critical deformations for control stability were upper plate radial and tangential bending. Lower plate deformations were not critical due to week interaction between upper and lower plate. The lowest resonance frequency of the bending modes was estimated to be greater than $f_0 = \omega_0/(2\pi) = 115$Hz and damping to be around $\zeta_0 \simeq 0.01$. Limiting the effect of bending and other modes to closed-loop stability and performance was a second major problem. Since digital control shall operate at a higher rate (1kHz) than f_0, structure deformations must be treated as part of the unmodeled dynamics and therefore can not be compensated by closed-loop control. As a consequence, structure vibration modes, excited by basement acceleration, were expected to yield the major contribution to control error. A simple evaluation of their effects can be obtained by assuming a white noise to drive a single mode centered at f_0. The root-mean-square (RMS) contributions σ_0 and $\underline{\sigma}_0$ to control error e and to its moving average $\underline{e}$ are estimated by

$$\sigma_0 = \frac{\underline{S}_a}{2\omega_0\sqrt{\zeta_0\omega_0}} \simeq 600pm, \underline{\sigma}_0 = \frac{\sigma_0}{A} \simeq 2.5pm \qquad (5)$$

where $A = 0.5\tau_0\omega_0 \simeq 240$ is the attenuation of the frequency components $> 1/\tau_0$ due to moving average. Since the effects of structural modes shall not be attenuated by closed-loop control, the above values must be well below, as they are, the FPI linear range ($\Delta_{max} = 2.5$nm) and the target average repeatability

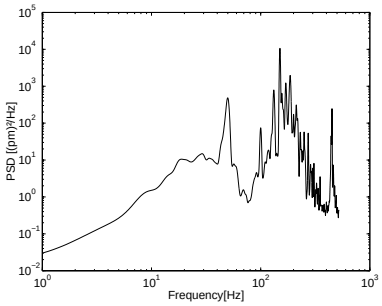

Figure 6: The PSD of the control error of a single cavity.

($\underline{\sigma}_e < 10$pm). Figure 6 shows the experimental PSD of the control error of a single cavity. The low-frequency band where PSD decreases corresponds to the closed-loop bandwidth ($\simeq 20$Hz). Figure 6 shows that structure resonance peaks are beyond the expected limit f_0 except for a pair of peaks due to electronic noise and a bending mode not affecting stability.

3 Digital control design

3.1 Design guidelines and architecture

Control design guidelines are the following. (i) To provide the actuated displacement of each upper reflector z_u with a sufficient resolution in response to thermo-elastic deformations (2), a control rate $f_c = 1$kHz and a command resolution $\rho_u \simeq 20$pm were proved to be sufficient. (ii) To attenuate aliasing of the wide-band acceleration noise, a simple digital anti-aliasing filter operating in two-rate mode was adopted.(iii) To simplify control algorithms, decoupling was assumed: the optical length of each FPI was independently controlled, by actuating the PZT translator near its upper reflector. Cross-coupling effects ($< 20\%$) were treated as unknown disturbances. (iv) To guarantee target repeatability (1), each FPI must be locked within its linear range. A supervisor performs this task.

Since DCU works in two-rate mode, two different discrete times must be defined: (i) the time kT_y of all FPI measures acquired at a rate $f_y = 1/T_y = 8$kHz, (ii) the time iT_c of the control commands actuated at a rate $f_c = f_y/N, N = 8$. The relation between k and i can be written as $k(i) = iN$. We denote also with $\widetilde{y}(k)$ a digital measure, output of a 16-bit Analog-to-digital converter sampling the FPI voltage signal $V(t)$ and with $\widetilde{u}(i)$ the digital command transmitted to an 18-bit digital-to-analog converter. DCU is the parallel of the three equal single-input-single-output (SISO) controllers each stabilizing a single cavity j (the term *cavity* will indicate hereafter one of the three Degrees-of-Freedom to be stabilized in distance). Each controller performs three main tasks. (i) *Anti-aliasing filter*: raw measurements $\widetilde{y}(k)$ are first sampled and filtered at the rate f_y. The filtered measures, sampled again at the control rate are the 'true' control measures $y(i)$. The main objective was to reduce as much as possible control rate (in view of space constraint) while keeping the same performance provided by a higher rate. (ii) *Feedback controller*: the filtered measure $y(i)$ supplies a state observer and then a feedback law which computes the voltage command $\widetilde{u}(i)$ driving each PZT. (iii) *Supervisor*: it detects transitions from stabilization to recovery conditions and vice versa (not treated here).

3.2 The design model and the anti-aliasing filter

The second design step aims at developing the *design model*, a set of simplified discrete-time state equations for designing control strategies. Decoupling assumption and test-bed symmetry imply that the SISO dynamics relating the real-valued command $u(i)$ to the real-valued measure $y(k)$ of each cavity have the same equations (subscript j will be usually omitted). The design model of each cavity is the result of the following simplifying assumptions. (i) The command $u(i)$ is kept constant during each control step i defined by $k = k(i) + h, h = 0, \ldots, N-1$ and $u(k) = u(i)$. (ii) The inertial displacement $z_u(k)$ of each upper reflector is proportional to the PZT voltage command $u(k)$ up to a disturbance term $d_u(k)$, i.e. $z_u(k) = b_j u(k) + d_u(k)$, where the open-loop gain b_j[m/V] is typical of each cavity. Proportionality follows by treating PZT dynamics and structure vibration modes as unmodeled dynamics and cross-coupling effects as an unknown disturbance $d_u(k)$. (iii) Within FPI linear range, the control error $e(k)$, expressed in length units, is equal to cavity detuning and therefore is proportional to upper and lower plate displacements through equation

$$e(k) = b_j u(k) + z_l(k) + d_u(k) + \eta_k = b_j u(k) + d(k) \quad (6)$$

where the lower plate displacement z_l, the measure error η and the upper plate disturbance d_u have been collected in a single disturbance d. (iv) The unknown disturbance $d(k)$ is modeled as the sum of a discrete-time white noise $w(k)$ and of a 2nd-order random drift $z(k)$ describing the low frequency components to be compensated by control action. Specifically $z(k)$ describes the rigid body motion of the lower plate subject to a white noise $a(k)$ accounting for basement acceleration and thermo-elastic deformations. (v) Anti-aliasing is realized by a first-order adder: $x(k+1) = x(k) + e(k)$, $x(0) = 0$, where the control error $e(k) = h_j(\widetilde{y}(k))$ is obtained by converting the digital measure $\widetilde{y}(k)$ into length units. The state $x(k)$, sampled at control rate, provides the 'true' control measure $y(i) = x(iN)$. The above assumptions and equations can be collected in the design state equation, sampled at control step i, one for each cavity:

$$\begin{aligned} \mathbf{x}(i+1) &= A\mathbf{x}(i) + Bu(i) + G\mathbf{w}(i),\ \mathbf{x}(0) = \mathbf{x}_0 \\ y(i) &= C\mathbf{x}(i) + \partial P(y_0(\mathbf{u}), a),\ y_0(i) = C\mathbf{x}(i) \quad (7) \\ e(i) &= H\mathbf{x}(i) + b_j u(i) + w(i), H = \left| 0\,1\,0 \right|, \end{aligned}$$

where

$$\left|\begin{array}{c|c|c} A & B & G \\ \hline C & & \end{array}\right| = \left|\begin{array}{ccc|c|cc} 1 & 1 & 0 & b_j & 1 & 0 \\ 0 & 1 & 1 & 0 & 0 & 0 \\ 0 & 0 & 1 & 0 & 0 & 1 \\ \hline 1 & 0 & 0 & & & \end{array}\right|, \ \mathbf{x} = \left|\begin{array}{c} x \\ z \\ v \end{array}\right| \quad (8)$$

The vector $\mathbf{x}(i)$ is the model state and $\mathbf{w}(i)$ includes the white noises $w(i)$ and $a(i)$. The pair (C, A) is observable, the pair (A, G) is controllable. The pair (A, B) is not stabilizable because disturbance dynamics has a pair of unitary eigenvalues. The operator ∂P, forced by the vector $\mathbf{u}$ of all commands u_j and by the acceleration noise a, accounts for the unmodeled dynamics and is added to the output $y_0(i)$ of the design model as an additive disturbance. Control design was fully developed around state equation (7).

3.3 Control algorithm - the state observer

As a third step the state observer of (7) is designed. Let us denote with $\widehat{e}(i) = y(i) - \widehat{y}(i)$ the observer output error and with $\widehat{\mathbf{w}}(i) = GL\widehat{e}(i)$ the observer correction vector. The key design maneuver is to constrain the correction vector $\widehat{\mathbf{w}}(i)$ to lay in the two-dimensional range of G: $\widehat{w}_2(i) = 0$. The constraint has the effect of improving observer performance Theorem 4 will show. Accordingly observer state equations become

$$\begin{aligned} \widehat{\mathbf{x}}(i+1) &= A\widehat{\mathbf{x}}(i) + Bu(i) + GL(y(i) - C\widehat{\mathbf{x}}(i)) \quad (9) \\ \widehat{y}(i) &= C\widehat{\mathbf{x}}(i), \ \widehat{\mathbf{x}}(0) = \widehat{\mathbf{x}}_0 \end{aligned}$$

Constraining observer corrections imposes limits to eigenvalue assignment and may jeopardize observer stability. To recover arbitrary assignment, a dynamic state correction $\widehat{\mathbf{w}}(i) = GL\widehat{e}(i) + GM\mathbf{q}(i)$ must be adopted, where $\mathbf{q}(i)$ is a suitable state vector driven by the observer output $\widehat{e}(i)$. The following theorem summarizes such results; the proof following directly from the characteristic polynomials of the observer state matrices.

Theorem 1 .(i) No gain vector L exists in (9) capable of assigning the eigenvalues of $A_o = A - GLC$ inside the unit disk. (ii) The least dimension of the state $\mathbf{q}(i)$ guaranteeing arbitrary eigenvalue assignment under the constraint $\widehat{w}_2(i) = 0$ equals 1. It implies that observer (9) modifies into a 4th-order state equation as follows

$$\begin{aligned} \left|\begin{array}{c} \widehat{\mathbf{x}} \\ q \end{array}\right|(i+1) &= \left|\begin{array}{cc} A_o & GM \\ -C & \lambda_0 \end{array}\right| \left|\begin{array}{c} \widehat{\mathbf{x}} \\ q \end{array}\right|(i) + \left|\begin{array}{c} B \\ 0 \end{array}\right| u(i) + \left|\begin{array}{c} GL \\ 0 \end{array}\right| y(i) \\ \widehat{y}(i) &= C\widehat{\mathbf{x}}(i), \ \left|\begin{array}{c} \widehat{\mathbf{x}} \\ q \end{array}\right|(0) = \left|\begin{array}{c} \widehat{\mathbf{x}}_0 \\ q_0 \end{array}\right|. \quad (10) \end{aligned}$$

The non zero gains of GL and of GM and the open-loop eigenvalue λ_0 of the state $q(i)$ are computed by assigning the 4th-order eigenvalue set Λ_o to the unit disk. According to [3], the eigenvalue set Λ_o shall not be assigned for minimizing the observer error covariance, but for blocking the effect of the unmodeled dynamics ∂P through the feedback chain and consequently for guaranteeing closed-loop stability and performance.

3.4 Control algorithm - the feedback control

At the fourth design stage the feedback control law is designed by neglecting the unmodeled dynamics ∂P and such as to force the controllable state $x(i)$ and the control error $e(i)$ to zero. The simple feedback law results: $u(i) = -(k\widehat{x}(i) + \widehat{z}(i))/b_j = -K\widehat{\mathbf{x}}(i)/b_j$, where the control gain k is bounded by $0 < k \leq 1$ and $K = |k\,1\,0|$. Such a law shows that $e(i)$ is chiefly forced to zero by compensating the disturbance term $d(i)$ through the observer estimate $\widehat{z}(i)$. Zero values will be only reached in the average because of noise and estimation errors. Internal stability of the closed loop state equation is assured by Theorem 2, proved by the characteristics polynomial of the state matrix.

Theorem 2 . Under the assumption that (i) the gain k is bounded by $0 < k \leq 1$, (ii) the estimation error $\widehat{\mathbf{e}}(i) = \widehat{\mathbf{x}}(i) - \mathbf{x}(i)$ is bounded and command independent, or in other words, that the unmodeled dynamics ∂P is neglected and the observer eigenvalue set Λ_o lies in the unit disk, the following closed-loop state equation is internally stable

$$\left|\begin{array}{c} x \\ \widehat{\mathbf{e}} \\ q \end{array}\right|(i+1) = \left|\begin{array}{ccc} 1-k & -K & 0 \\ 0 & A_o & GM \\ 0 & -C & \lambda_0 \end{array}\right| \left|\begin{array}{c} x \\ \widehat{\mathbf{e}} \\ q \end{array}\right|(i) + \left|\begin{array}{c} KG \\ -G \\ 0 \end{array}\right| \mathbf{w}(i) \quad (11)$$

3.5 Control algorithm - observer eigenvalues

When the measure $y(i)$ is obtained from the 'real plant', Theorem 2 assumption ceases to be valid because of the unmodeled dynamics ∂P. Its effect spills through plant measure $y(i)$ by making the estimation error command-dependent through an uncertain dynamic operator $\widehat{\mathbf{e}} = \widehat{\mathbf{E}}_x(y_0(\mathbf{u}), a)$. To be simple, only the operator $\mathbf{E}_x$ mapping the model output $y_0 = x$ to the first component of the estimation error $\widehat{e}_0 = y_0 - \widehat{y}$ will be considered. $\mathbf{E}_x$ can be alternatively expressed as $\widehat{e}_0 = \mathbf{E}_x(y_0(\mathbf{u}), a) = V_o(\partial P(y_0(\mathbf{u}), a)$, where V_o is the linear dynamic operator of the observer (10) mapping the FPI measure y into the estimate $\widehat{y}$. According to [3], a way to recover Theorem 2 and to guarantee closed-loop stability in presence of uncertain dynamics, is to assign the observer eigenvalue set Λ_o the unit disk in such a way to bound the effect of $\mathbf{E}_x$ on the state estimation error $\widehat{e}_0$.

Theorem 3 [3]. If the observer operator V_o guarantees that the $\mathbf{E}_x$ satisfies the norm inequality

$$|\widehat{e}_0| < E_x|y_0| + E_0, \ E_x < 1, \ E_0 < \infty, \quad (12)$$

the feedback control designed by neglecting the unmodeled dynamics ∂P, stabilizes both the closed-loop equation (11) and the ensemble 'plant+observer' mapping the command vector $\mathbf{u}$ to $\widehat{y}$.

E_x is the norm of the operator $\mathbf{E}_x$ and E_0 is a bound to command-independent effects. Inequality (12), although sufficient to recover stability, is not sufficient

to recover the model-based performance guaranteed by Theorem 2. It can be recovered by lowering E_x and E_0. Because inequality (12) cannot be guaranteed analytically, the simulated fine model provides a friendly test-bed of the critical and uncertain dynamics, where to a priori guarantee stability and performance. Experience shows that the risk of in-field degradation becomes very low: COSI test-bed was finalized by running digital control and as soon as discrepancies with respect to model assumptions, due to not finalized optics, were eliminated, digital control achieved the target performance. Analytic computation of E_x and E_0, made by a simple model of ∂P, may provide starting values of the control parameters to be refined by simulated runs and a way to compare different observers as Theorem 4, given without proof, states.

Theorem 4 . Let us assume that (i) ∂P is modeled by a single vibration mode, $f_0 = 115$Hz, $\zeta_0 = 0.01$, (ii) all observer eigenvalues are equal to $|\lambda| < 1$ and (iii) an H_∞ norm is adopted for $\mathbf{E}_x$. Then E_x has the following expression

$$E_x = \frac{1}{2\zeta_0}\left(\frac{3f_c|1-\lambda|}{2\pi f_0}\right)^m < 1 \qquad (13)$$

where $m = 2$ for the constrained observer (10) and $m = 1$ for the unconstrained one. In turn equation (13) provides a lower limit λ_{min} to observer eigenvalues λ, i.e. $\lambda_{min} = 0.96$ for the constrained observer and the very conservative limit $\lambda_{min} = 0.995$ for the unconstrained one.

Refinement through simulator, confirmed by in-field runs, proved that the less conservative range $0.9 \leq \lambda \leq 0.96$ of the observer eigenvalues was guaranteeing target performance. To conclude, the control algorithm, valid under stabilization conditions, is a 5th-order dynamic feedback law for each cavity, including a 1st order anti-aliasing filter, a 4th order state observer and a static feedback law.

4 Experimental results and conclusions

Two main series of tests were performed, limited in time duration to 11 minutes due to static vacuum conditions. (i) *Environment tests.* Only basement acceleration noise acted on the test-bed. Tests allowed to measure the RMS of the not compensated structural vibrations (beyond the 20Hz control bandwidth) and to verify that control error was kept within the FPI linear range at least during quiet day hours. (ii) *Thermo-elastic deformation tests.* Lower plate actuators (high voltage PZTs) were periodically excited according to requirements (2). Table 1 shows the results of both tests (environment test results are in brackets). In the thermo-elastic test emulating tilt deformation, only cavity 1 and 3 were excited at an amplitude of 0.5μm and a maximum rate of 0.1μm/s.

Table 1 - Test results: Saturday morning, 11m (11s) duration

RMS [pm]	Target	Cavity 1	Cavity 2	Cavity 3
Control error σ_e	<600	150(140)	240(280)	590 (380)
Average error $\underline{\sigma}_e$	<10	0.7(0.5)	0.8(0.8)	2.3(1.1)
Attenuation A	260	215(280)	300(350)	255(345)

Performance differences among cavities are mainly due to a dissimilar response of the structural modes to basement acceleration. Note however that attenuation A is

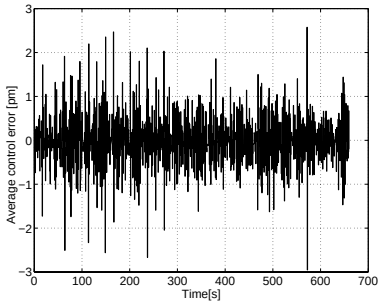

Figure 7: The moving average of the cavity 1 control error

quite similar and larger than predicted by equation (5). In the thermo-elastic test A decreases because of the additional noise due to command resolution in response to deformation rate. Figure 7 shows the average control error of cavity 1 during thermo-elastic test.

The above results confirm that target performance was widely met reaching pm repeatability over 1s time scales. COSI test-bed is a 'unique' instrument deploying leading measure and control technology for sub-nanometric stabilization and metrology. Developments concern digital control application to laser frequency stabilization and to ultra-stable reference cavities.

References

[1] Bava E. and Massari F. "Phase sensitive detection of light reflected by a Fabry-Perot interferometer", *Rev. Sci. Instrum.*, 67 (1996), p. 1714-1720.

[2] Bisi M. and Bertinetto F. "Frequency reproducibility of He-Ne lasers at lλ=612nm using the frequency modulation spectroscopy technique", *Metrologia*, 34 (1997), p. 451-457.

[3] Donati F. and Vallauri M. "Guaranteed cost control of uncertain dynamic systems", *IEEE Trans. Autom. Control*, 29 (1984), p. 34-41.

[4] Drever R. W. et al. "Laser phase and frequency stabilization using an optical resonator", *Appl. Phys. B*, 97 (1983).